Int. J. of Thermal & Environmental Engineering
Volume 21, No. 1 (2024) 01-05

Experimental and Computational Investigation of Jet Impingement Cooling for Gas Turbine Blades

Mohammed Aldhaheri [a], Khamis Humaid [a], Abdulraman Al-Ali [a], Adel Sumjath [a]

[a] *Department of Mechanical Engineering, Khalifa University of Science and Technology, Abu Dhabi, UAE*

Abstract

Gas turbines are widely used in power generation and aviation industries due to their high efficiency and reliability. However, their performance is significantly affected by thermal loads, making effective cooling strategies essential for maintaining operational integrity. This study explores state-of-the-art cooling techniques for gas turbine components, focusing on impingement jet cooling. Computer Fluid Dynamics (CFD) as well as experiments were performed to test the effect of mass flow rate, inlet jet width and its position on the cooling performance. Three key parameters were examined: average cavity wall temperature, outlet temperature, and the average Nusselt number. The model was exposed to a continuous heat flux and the cavity temperature measurements were recorded. Results indicated that the lowest average cavity wall temperature was achieved at the smallest inlet width and highest mass flow rate, with mass flow rate as the most significant factor.

Keywords: *Gas turbines, Jet impingement Cooling, Turbine efficiency, CFD, Heat transfer enhancement*

1. Introduction

Gas turbines are essential in industries such as power generation, aviation, and oil and gas, where high efficiency, reliability, and safety are paramount. The performance and lifespan of a gas turbine significantly impact its overall operational cost and economic viability [1]. A gas turbine is a rotating thermal engine that converts energy from combusted fuel into mechanical power. It is known for its high reliability, low emissions, and considerable electrical efficiency [2].

Turbine blades operate under extreme conditions, being exposed to high temperatures, pressures, and chemically aggressive environments [3]. These harsh conditions contribute to various degradation mechanisms, including fatigue, creep, corrosion, erosion, foreign object damage, and vibration, which can compromise blade integrity [4]. Carter [5] highlighted that prolonged high-speed operation exacerbates these issues, leading to failures in critical components such as compressors, combustors, and vanes. Early blade fractures are a primary cause of turbine failures, resulting in unplanned shutdowns and substantial financial losses [6]. Additionally, Cao et al. [7] emphasized that in some turbine designs, component failures necessitate the replacement of the entire system, further increasing costs and downtime. Consequently, improving gas turbine performance and durability has become an area of growing importance [8].

A study by Kanesund et al. [9] examined various operational challenges, identifying pitting corrosion as one of the most critical issues affecting turbine blades. This localized form of corrosion weakens structural integrity and serves as an initiation site for fatigue cracks, accelerating component failure. Corrosion also accelerates crack propagation due to its temperature-dependent nature. Furthermore, experimental research by Wang et al. [10] demonstrated that turbine failures often result from multiple interacting failure mechanisms, such as the simultaneous effects of creep and fatigue. The interaction between these two factors is particularly detrimental at high temperatures, where prolonged stress leads to microstructural degradation, reducing the material's resistance to cyclic loading. Mirhosseini et al. [11] underscored the necessity of detailed failure analysis to identify the root causes of blade failures and improve turbine reliability. While protective coatings can mitigate early-stage corrosion, they provide only a temporary solution, as they degrade over time due to thermal cycling, oxidation, and mechanical wear, necessitating frequent reapplication and maintenance [12].

Future advancements in gas turbine technology emphasize the need for effective cooling strategies to enhance efficiency and durability. Gas turbine blade cooling is one of the most influential factors in improving turbine efficiency [13]. Effective cooling techniques help maintain structural integrity and extend blade lifespan by allowing higher operating temperatures without compromising material performance. Blade cooling techniques are broadly categorized into internal and external methods [14]. Internal cooling involves jet impingement cooling, where relatively cool air from the compressor is forced through internal blade passages to dissipate heat effectively [15]. Advances in serpentine cooling channel designs have significantly improved internal cooling efficiency. However, internal cooling alone is often insufficient to protect blades from extreme thermal loads, necessitating external cooling solutions [16].

External cooling methods, such as film cooling, transpiration cooling, and effusion cooling, play a crucial role in thermal protection [17]. Film cooling, one of the most widely used techniques, injects coolant through small holes or slots on the

* Corresponding author. Tel.:
E-mail:

DOI: 10.5383/ijtee.21.01.001

blade surface, creating a thin insulating layer that reduces direct heat transfer from hot combustion gases. Effusion cooling, a more advanced approach, utilizes a dense array of micro-perforations to generate a uniform cooling film, improving thermal resistance and overall efficiency. The effectiveness of these cooling techniques depends on parameters such as hole arrangement, injection angle, and coolant properties, all of which significantly impact turbine blade performance and longevity.

Computational Fluid Dynamics (CFD) has become an invaluable tool for analyzing turbine performance, enabling researchers to simulate airflow, heat transfer, and operational conditions with high accuracy [18]. Leidenberger and Urban [19] highlighted the widespread application of CFD in fields such as automotive, shipbuilding, and turbine optimization, where even minor efficiency improvements yield significant economic benefits. CFD-driven advancements have led to substantial improvements in turbine blade designs and cooling methodologies [20]. Ali and Janajreh [21] conducted a numerical study on jet impingement cooling of a semi-circular surface, comparing central and side jet configurations. They found that central jets offered more effective localized cooling, and shorter jet-to-surface distances enhanced heat transfer. When applied to turbine blades, the optimized jet setup significantly reduced surface temperatures and improved thermal performance.

This study involves a novel approach to turbine blade cooling by optimizing jet impingement. Our study focuses on validating the effectiveness of jet cooling simulation through an experiment. The experimental results confirm the practical application of jet impingement cooling, providing valuable insights into its potential to enhance turbine blade thermal protection, efficiency, and longevity.

2. Methodology

2.1. Governing Equations

The Reynolds-Averaged Navier-Stokes (RANS) equations form the foundation of CFD for modeling turbulent flows. RANS simplifies turbulence modeling by decomposing the velocity field into a time-averaged and fluctuating component, reducing computational complexity while retaining essential flow characteristics. This approach enables the efficient simulation of a wide range of fluid dynamic applications, from small-scale turbulent mixing in microchannels to large-scale engineering challenges, such as gas turbine performance and aircraft aerodynamics [22]. RANS-based simulations offer a practical balance between computational efficiency and predictive capability. However, while RANS models perform well for many industrial applications, they may be less accurate in flows involving strong separation, high unsteadiness, or complex turbulent structures, where higher-fidelity models such as Large Eddy Simulation (LES) or Direct Numerical Simulation (DNS) may be required [23]. In this work, RANS equations with *k-ω* turbulence modeling are used, as given below.

Continuity equation:

$$\frac{\partial}{\partial x_i}(\rho u_i) = 0 \quad (1)$$

where ρ is the density of the fluid, and u_i is the axial velocity.

Momentum equation:

$$\frac{\partial}{\partial x_j}(\rho u_i u_j) = -\frac{\partial \rho}{\partial x_i} + \frac{\partial}{\partial x_j}\left[\mu\left(\frac{\partial u_i}{\partial x_j} + \frac{\partial u_j}{\partial x_i} - \frac{2}{3}\delta_{ij} + \frac{\partial u_i}{\partial x_j}\right)\right] + \frac{\partial}{\partial x_j}(-\rho\overline{u_i' u_j'}) \quad (2)$$

where μ represents the dynamic viscosity of the fluid, u_i denotes the axial velocity, and u_j' signifies the fluctuating velocity. The turbulent shear stress is expressed as $(-\rho\overline{u_i' u_j'})$.

Energy equation:

$$\frac{\partial}{\partial x_j}[u_j(\rho E + P)] = \frac{\partial}{\partial x_j}\left[\left(K + \frac{C_p \mu_t}{Pr_t}\right)\frac{\partial T}{\partial x_j} + u_i(\tau_{ij})_{eff}\right] \quad (3)$$

where P represents pressure, K the thermal conductivity, and E denotes the total energy. On the right-hand side of the equation, Cp is the specific heat at constant pressure, μ_t is the turbulent viscosity, Pr_t is the turbulent Prandtl number, and $(\tau_{ij})_{eff}$ is the deviatoric stress tensor.

Turbulence kinetic energy:

$$\frac{\partial(\rho k)}{\partial t} + \frac{\partial(\rho u_j k)}{\partial x_j} = \rho P - \beta\rho\omega k + \frac{\partial}{\partial x_j}\left[\left(\mu + \sigma_k \frac{\rho k}{\omega}\right)\frac{\partial k}{\partial x_j}\right] \quad (4)$$

where k is the turbulence kinetic energy, and ω is the specific dissipation rate. The term $\beta\rho\omega k$ accounts for turbulence dissipation, and the last term models the diffusion of turbulence energy, where σ_k is an empirical constant.

Specific rate of dissipation:

$$\frac{\partial(\rho\omega)}{\partial t} + \frac{\partial(\rho u_j \omega)}{\partial x_j} = \frac{\gamma\omega}{k} P - \beta\rho\omega^2 + \frac{\partial}{\partial x_j}\left[\left(\mu + \sigma_\omega \frac{\rho k}{\omega}\right)\frac{\partial \omega}{\partial x_j}\right] + \frac{\rho\sigma_d}{\omega}\frac{\partial k}{\partial x_j}\frac{\partial \omega}{\partial x_j} \quad (5)$$

2.2 Numerical Methodology

A computational simulation of jet cooling in turbine blades was conducted using ANSYS Fluent. The study examined three key parameters: average cavity wall temperature, outlet temperature, and the average Nusselt number of the cavity wall. These variables were influenced by three factors: mass flow rate, inlet width, and inlet height. Four mass flow rates were determined by using velocities at constant density and area ($\dot{m} = \rho A v$). The four mass flow rates: 0.003, 0.006, 0.012, and 0.024 kg/s. Inlet widths of 0.125 cm, 0.25 cm, 0.5 cm, and 1 cm were considered, along with four inlet positions: top, quarter, half, and three-quarter depth. This resulted in a total of 64 simulation cases. The objective was to identify configurations that yielded the lowest average cavity wall temperature and the highest Nusselt number, indicative of optimal heat transfer efficiency.

The simulation was conducted with well-defined thermal and flow boundary conditions to ensure accurate representation of jet cooling performance. A fixed inlet temperature of 300 K was applied, with velocity varying according to each case as shown in Fig. 1. The outlet was defined as a pressure outlet with 0 Pa (gauge). The cavity wall was subjected to a uniform heat flux of 10,000 W/m², while the top wall was treated as an adiabatic boundary with no heat flux. These conditions ensured a controlled thermal environment for evaluating jet cooling performance.

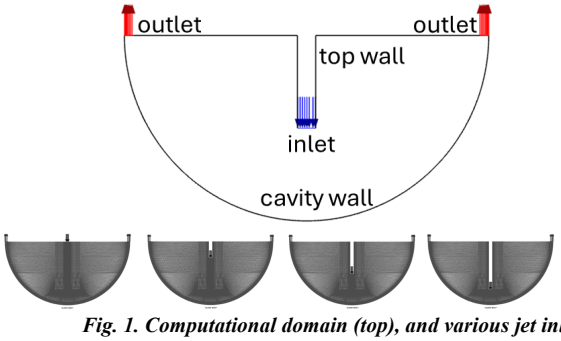

Fig. 1. Computational domain (top), and various jet inlet positions (bottom).

The simulation was based on several assumptions:

- The fluid density was assumed to be constant with a fixed inlet velocity.
- Heat transfer across boundaries was considered uniform.
- A simplified geometric model was used.

2.2.1 Mesh Sensitivity

A mesh sensitivity analysis was conducted using a baseline configuration:

- Inlet width = 0.5 cm

- Velocity = 1 m/s
- Inlet position = top

A mesh sensitivity was carried out and the results are summarized in Table 1.

Table 1. Mesh sensitivity analysis for different mesh configurations.

Mesh Designation	Relative Error in Cavity Temperature and Nusselt Number
Fine	-
Baseline	0.25%; 1.04%
Coarse 1	0.39%; 1.29%
Coarse 2	0.62%; 2.58%

2.3 Experimental Methodology

The primary goal of the experiment was to validate the numerical results. The key difference between the CFD and the experiment is that the simulation was conducted on a two-dimensional (2D) domain, whereas the experiment was three-dimensional (3D).

The experiment involved a 3D metal piece made of aluminum that was subjected to continuous heat input at the cavity using a heat flux. Once a constant temperature was achieved at the cavity, airflow was introduced through the center. For the exits, rectangular slots were chosen to ensure consistent airflow. The objective was to observe the temperature gradient before and after introducing air to the cavity. The experiment tests four different airflow velocities and four varying heights, starting from the surface of the cavity and going deeper into it. Fig. 2 shows a schematic representation of the experimental model, and Fig. 3 shows the 3D CAD model.

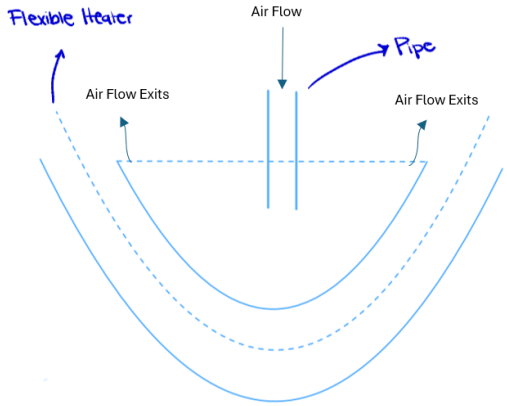

Fig. 2. A simple schematic of the experimental model showing the cross-section of the blade.

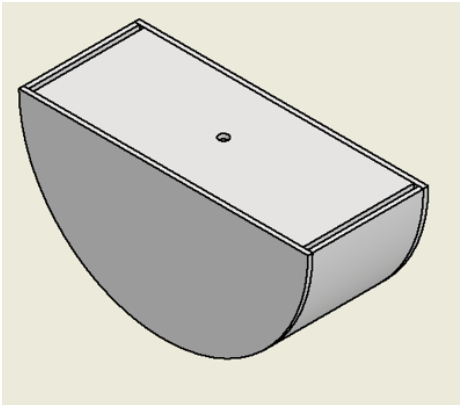

Fig. 3. CAD model of the cavity used for the experiment.

The experiment began with the placement of four thermocouple sensors inside the cavity to measure temperature. These sensors were connected to a data acquisition system, and a custom program was developed to display the temperature of the sensors. The experimental setup is shown in Fig. 4.

Heaters were placed on the exterior of the cavity to provide constant heat flux. To minimize the heat loss, the cavity was insulated using a thick rubber sheet. The heaters were powered by a DC power supply, which was set to a specific voltage and current to deliver the required heat flux to the cavity.

The top metal piece of the model was secured, and silicone was applied to the edges to prevent air leaks. An airflow meter was used to measure the mass flow rate of air entering the model. The velocity of the airflow was calculated using the following equations:

$$\dot{m} = \rho \cdot A \cdot v \tag{6}$$

$$\dot{m} = \rho \cdot \frac{\pi \cdot D^2}{4} \cdot v \tag{7}$$

$$v = \frac{4 \cdot \dot{m}}{\pi \cdot \rho \cdot D^2} \tag{8}$$

where $\dot{m}$ is the mass flow rate, ρ is air density, and D is the pipe diameter used to supply air. Clips were used to ensure no air leaked from the pipe.

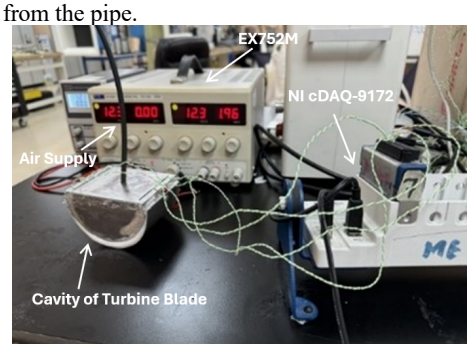

Fig. 4. Experimental setup.

3. Results and Discussion

3.1 Numerical Results

Figs. 5 and 6 present the simulation results, illustrating the influence of inlet width, height, and mass flow rate on average cavity temperature distribution. At lower mass flow rates, both inlet width and height significantly affected the temperature distribution. Narrower inlets and jet positioning closer to the cavity wall resulted in lower temperatures due to improved local cooling. However, at higher mass flow rates, the inlet width emerged as the dominant factor, exerting a greater influence on temperature reduction compared to inlet positioning.

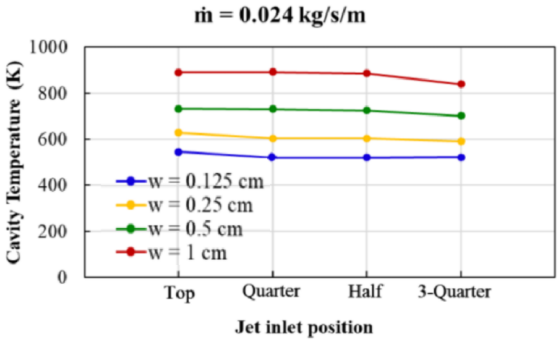

Fig. 5. Average cavity temperature at mass flow rate of 0.024 kg/s.

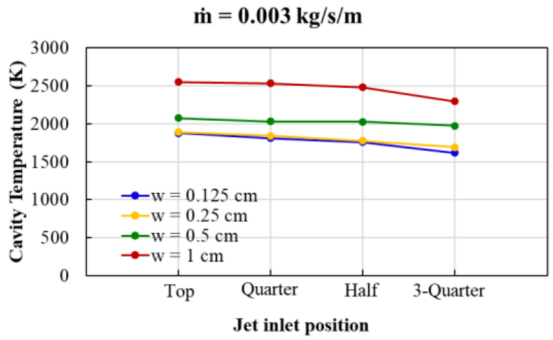

Fig. 6. Average cavity temperature at mass flow rate of 0.003 kg/s.

Fig. 7 shows the temperature contours for different configurations at velocity of 2 m/s and jet inlet width of 0.125 cm. The simulation results indicate that the lowest average cavity wall temperature was achieved with the smallest inlet width and highest mass flow rate, regardless of inlet height. Mass flow rate was the most significant factor in reducing cavity temperature, particularly when the inlet was positioned at the top. The increase in mass flow rate also correlated with a rise in the Nusselt number, highlighting enhanced heat transfer.

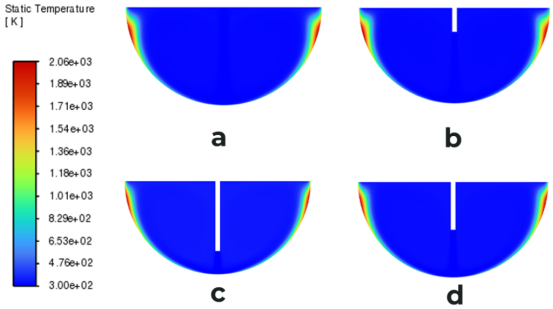

Fig. 7. Temperature contours at different jet inlet positions: (a) top, (b) quarter, (c) half, and (d) three-quarter, respectively.

A coefficient analysis was performed to quantify the influence of mass flow rate (A), jet inlet width (B), and jet inlet position (C) on average cavity wall temperature, as shown in Fig. 8. The results confirm that mass flow rate exerts the greatest influence, followed by inlet width.

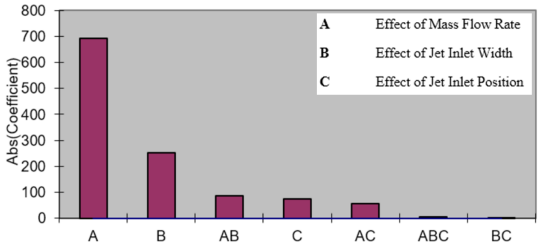

Fig. 8. Effect of each parameter on the average cavity wall temperature.

3.2 Experimental Results

The experiment was conducted at four different heights and four mass flow rates totaling 16 runs. Fig. 9 shows the effect of mass flow rate and inlet position on the average cavity wall temperature.

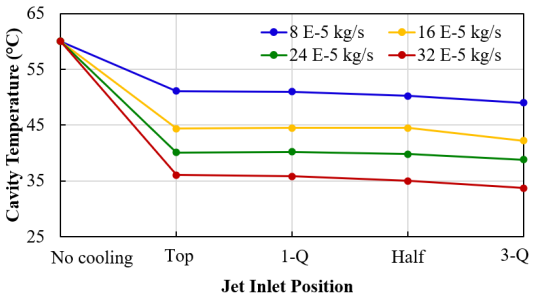

Fig. 9. Effect of mass flow rate and inlet position on the average cavity wall temperature.

In the absence of cooling, the cavity temperature remained steady at approximately 60°C. Since a constant heat input was applied and no airflow was present to dissipate the heat, the temperature remained stable. Once airflow was introduced through the central pipe at a mass flow rate of 8E-5 kg/s, the temperature began to decrease, reaching approximately 50.3°C across all depths. The depth closest to the cavity exhibited the lowest temperature, around 49°C.

After achieving a stable temperature at this mass flow rate, the airflow was increased to 16E-5 kg/s. A further temperature reduction was observed, with an average temperature of 43.9°C, while the three-quarter depth recorded the lowest temperature at 42.2°C. When the mass flow rate was increased to 24E-5 kg/s, the temperature reached a minimum of 38°C, with an average of 39.7°C. At the highest tested mass flow rate of 32E-5 kg/s, the mean temperature decreased to 35.1°C, while the closest depth to the cavity exhibited the lowest temperature at 33.7°C.

Fig. 9 highlights two key findings from this experiment. First, increasing the mass flow rate significantly reduces the cavity temperature. Higher airflow enhances cooling effectiveness, as evidenced by the temperature drop observed across the tested flow rates. Second, the depth of airflow relative to the cavity plays a crucial role in cooling efficiency. The three-quarter depth consistently recorded the lowest temperatures across all mass flow rates, demonstrating that proximity to the cavity improves cooling performance.

Additionally, it was observed that the initial mass flow rate (8E-5 kg/s) resulted in the most substantial temperature reduction. As the mass flow rate increased, the rate of temperature reduction became more gradual. These findings emphasize the importance of both mass flow rate and its proximity to the cavity in optimizing cooling performance, offering valuable information for practical applications in gas turbine blade cooling and thermal management systems.

4. Conclusion

Effective cooling is a critical factor in gas turbine operation, ensuring durability and efficiency under extreme thermal conditions. This study investigated the implementation of jet impingement as an impactful cooling technique for turbine blades. Both numerical simulations and experimental analyses were conducted on a semi-circular concave cross-section of the blade. The effects of mass flow rate, inlet width, and inlet position on the heat transfer performance were evaluated. The average cavity wall temperature and Nusselt number were recorded. The results concluded that mass flow rate had the most influence on average cavity wall temperature among all parameters. A direct inverse proportional relation is obtained, where average cavity wall temperature decreased significantly as mass flow increased. Future research should focus on integrating adaptive cooling mechanisms and AI-driven

optimization techniques to further improve gas turbine efficiency. By refining cooling strategies, the industry can achieve better fuel efficiency, reduced emissions, and longer operational life for gas turbines.

Nomenclature

D	Diameter, m
T	Temperature, K or ℃
P	Pressure, Pa
E	Total energy
ρ	Mass density, kg/m^3
A	Area, m^3
$\dot{m}$	Mass flow rate, kg/s
v	Velocity, m/s
u_i	Axial velocity, m/s
μ	Dynamic viscosity, Pa-s
u_j'	Fluctuating velocity, m/s
u_t	Turbulent viscosity, Pa-s
Pr_t	Turbulent Prandtl number
k	Turbulence kinetic energy, m^2/s^2

References

[1] P. Biswal, M. R. P., and C. Balaji, "Research advances on mist assisted impingement and film cooling of turbine blades," International Journal of Heat and Mass Transfer, vol. 232, p. 125907, Nov. 2024, doi: 10.1016/j.ijheatmasstransfer.2024.125907.

[2] T. S. Chowdhury, F. T. Mohsin, M. M. Tonni, M. N. H. Mita, and M. M. Ehsan, "A critical review on gas turbine cooling performance and failure analysis of turbine blades," *International Journal of Thermofluids*, vol. 18, p. 100329, May 2023, doi: 10.1016/j.ijft.2023.100329.

[3] P. Puspitasari, A. Andoko, and P. Kurniawan, "Failure analysis of a gas turbine blade: A review," *IOP Conf. Ser.: Mater. Sci. Eng.*, vol. 1034, no. 1, p. 012156, Feb. 2021, doi: 10.1088/1757-899X/1034/1/012156.

[4] G. H. Farrahi, M. Tirehdast, E. Masoumi Khalil Abad, S. Parsa, and M. Motakefpoor, "Failure analysis of a gas turbine compressor," *Engineering Failure Analysis*, vol. 18, no. 1, pp. 474–484, Jan. 2011, doi: 10.1016/j.engfailanal.2010.09.042.

[5] T. J. Carter, "Common failures in gas turbine blades," *Engineering Failure Analysis*, vol. 12, no. 2, pp. 237–247, Apr. 2005, doi: 10.1016/j.engfailanal.2004.07.004.

[6] M. García-Martínez, J. C. Del Hoyo Gordillo, M. P. Valles González, A. Pastor Muro, and B. González Caballero, "Failure study of an aircraft engine high pressure turbine (HPT) first stage blade," *Engineering Failure Analysis*, vol. 149, p. 107251, Jul. 2023, doi: 10.1016/j.engfailanal.2023.107251.

[7] Y. Cao, Y. Gao, Y. Zheng, and Y. Dai, "Optimum design and thermodynamic analysis of a gas turbine and ORC combined cycle with recuperators," *Energy Conversion and Management*, vol. 116, pp. 32–41, May 2016, doi: 10.1016/j.enconman.2016.02.073.

[8] P. A. Pilavachi, "Power generation with gas turbine systems and combined heat and power," *Applied Thermal Engineering*, vol. 20, no. 15–16, pp. 1421–1429, Oct. 2000, doi: 10.1016/S1359-4311(00)00016-8.

[9] J. Kanesund, H. Brodin, and S. Johansson, "High temperature corrosion influence on deformation and damage mechanisms in turbine blades made of IN-792 during service," *Engineering Failure Analysis*, vol. 110, p. 104388, Mar. 2020, doi: 10.1016/j.engfailanal.2020.104388.

[10] R. Wang *et al.*, "Thermomechanical fatigue experiment and failure analysis on a nickel-based superalloy turbine blade," *Engineering Failure Analysis*, vol. 102, pp. 35–45, Aug. 2019, doi: 10.1016/j.engfailanal.2019.04.023.

[11] A. M. Mirhosseini, S. Adib Nazari, A. Maghsoud Pour, S. Etemadi Haghighi, and M. Zareh, "Failure analysis of first stage nozzle in a heavy-duty gas turbine," *Engineering Failure Analysis*, vol. 109, p. 104303, Jan. 2020, doi: 10.1016/j.engfailanal.2019.104303.

[12] B. Swain *et al.*, "Failure analysis and materials development of gas turbine blades," *Materials Today: Proceedings*, vol. 33, pp. 5143–5146, 2020, doi: 10.1016/j.matpr.2020.02.859.

[13] M. Rajabinezhad, A. Bahrami, M. Mousavinia, S. J. Seyedi, and P. Taheri, "Corrosion-Fatigue Failure of Gas-Turbine Blades in an Oil and Gas Production Plant," *Materials*, vol. 13, no. 4, p. 900, Feb. 2020, doi: 10.3390/ma13040900.

[14] U. Ali and M. S. Kamran, "Geometric Optimization of a Gas Turbine Blade Cooling Passage using CFD," *International Journal of Thermal and Environmental Engineering (IJTEE)*, vol. 17, no. 2, pp. 105–114, 2020.

[15] A. S. J. Van Heerden, D. M. Judt, S. Jafari, C. P. Lawson, T. Nikolaidis, and D. Bosak, "Aircraft thermal management: Practices, technology, system architectures, future challenges, and opportunities," *Progress in Aerospace Sciences*, vol. 128, p. 100767, Jan. 2022, doi: 10.1016/j.paerosci.2021.100767.

[16] J.-C. Han, "Recent Studies in Turbine Blade Cooling," *International Journal of Rotating Machinery*, vol. 10, no. 6, pp. 443–457, Jan. 2004, doi: 10.1155/S1023621X04000442.

[17] S. Xue and W. F. Ng, "Turbine Blade Tip External Cooling Technologies," *Aerospace*, vol. 5, no. 3, p. 90, Aug. 2018, doi: 10.3390/aerospace5030090

[18] J. Tu, G. H. Yeoh, C. Liu, and Y. Tao, *Computational fluid dynamics: a practical approach*, Fourth edition. Oxford Cambridge, MA: Butterworth-Heinemann, 2024. doi: 10.1016/C2021-0-01771-5.

[19] R. Leidenberger and K. Urban, "Automatic differentiation for the optimization of a ship propulsion and steering system: a proof of concept," *J Glob Optim*, vol. 49, no. 3, pp. 497–504, Mar. 2011, doi: 10.1007/s10898-010-9609-6.

[20] Y. F. Gorgulu, "CFD-based cooling performance of gas turbine blades," *AEAT*, Mar. 2025, doi: 10.1108/AEAT-01-2025-0037.

[21] A. R. A. Ali and I. Janajreh, "Numerical Simulation of Turbine Blade Cooling via Jet Impingement," *Energy Procedia*, vol. 75, pp. 3220–3229, Aug. 2015, doi: 10.1016/j.egypro.2015.07.683.

[22] W. Rodi, "Comparison of LES and RANS calculations of the flow around bluff bodies," *Journal of Wind Engineering and Industrial Aerodynamics*, vol. 69–71, pp. 55–75, Jul. 1997, doi: 10.1016/S0167-6105(97)00147-5.

[23] I. Celik, "RANS/LES/DES/DNS: The Future Prospects of Turbulence Modeling," *Journal of Fluids Engineering*, vol. 127, no. 5, pp. 829–830, Sep. 2005, doi: 10.1115/1.2033011